

Pure blue light-emitting fluorene-based conjugated polymer with excellent thermal, photophysical, and electroluminescent properties

Cheng Yang · Hong-Song Song · Da-Bo Liu

Received: 3 April 2013 / Accepted: 23 May 2013 / Published online: 31 May 2013
© Springer Science+Business Media New York 2013

Abstract A functionalized polyfluorene (FPF) with dendritic carbazole and oxadiazole side chains have been successfully designed, synthesized, and characterized. The weight-average molecular weight (M_w) and number-average molecular weight (M_n) were measured by gel permeation chromatography (GPC) to be 71280 and 31185, respectively. The FPF is thermally stable with high decomposition temperature ($T_d = 495$ °C) and glass transition temperature ($T_g = 160$ °C), and show good solubility in organic solvents, such as *N,N*-dimethyl formamide, tetrahydrofuran, CHCl_3 , and toluene. The photoluminescent and electroluminescent (EL) emissions and Commission Internationale de L'Eclairage coordinates indicated pure blue light emission of FPF and its device. The luminance–voltage (L – V) and current density–voltage (J – V) characteristics of the devices based on FPF indicated typical diode characteristics with a maximum luminance of 980 cd/m^2 at a drive voltage of 13.0 V, a maximum current density of 726 mA/cm^2 , and a turn-on voltage of 8.54 V. The maximum EL efficiency of the device based on FPF was measured to be 0.46 % at the current density of 12.5 mA/cm^2 . These results indicate that the FPF polymer could be a promising candidate for pure blue light-emitting polymer with excellent thermal, photophysical, and electroluminescent properties.

Introduction

Conjugated polymers have attracted much attention because of their potential applications in polymer light-emitting diodes (PLEDs) [1–5]. The PLEDs based on conjugated polymers are considered as promising candidates for the next generation flat-panel displays and lighting applications. At present, the stability and life of red- and green-light devices has basically reached the practical requirements, but the brightness, stability, and life of blue-light device is still poor, so the performance of blue-light device remains to be further improved [6]. The development of blue light-emitting polymers has been the subject of academic and industrial research because of their potential applications in full-color displays. In particular, blue electroluminescent (EL) polymers with large band gap have been studied intensively, since they not only emit one of the three primary colors (red-, green-, and blue-light), but can also be used as host materials to realize emission covering whole visible region. Until now, the achievement of efficient and stable blue electroluminescence (EL) remains a great challenge on the path to PLED full-color displays [7–12]. Table 1 shows the achievements of already available reports on blue OLED/PLED [13–20].

Polyfluorene (PF) has emerged as a very promising material for blue EL because of its high photoluminescence (PL) quantum efficiency in the solid state, good thermal stability, good film-forming properties, and high processability [21–27]. However, PF based polymers are hole-transport-dominated materials, which exhibit low electron mobility in EL devices. PF-based polymers unbalanced charge injection, and transport properties limit the efficient recombination of holes and electrons, resulting in a decrease in EL efficiency [28–34]. Moreover, PF has a

C. Yang (✉) · H.-S. Song · D.-B. Liu
Department of Structural Steel, Functional Materials and Heat Treatment Processing, Beijing Institute of Aeronautical Materials, Beijing 100095, China
e-mail: chengyang_78@126.com

Table 1 The achievements of already available reports on blue OLED/PLED

Literatures	Time (year)	Works	Achievements
P. S. Vincett et al. [13]	1982	OLED of using anthracene as emitting layer at 30 V.	Blue-light intensity was very low, and the life was so short.
Chihaya Adachi et al. [14]	1990	OLED of using TPB as emitting layer at 30 V.	Blue-light intensity was 700 cd/m ² .
Ma Yu-guang et al. [15]	1994	OLED of using blends of TPD and PVK as emitting layer	The blue emission at 455 nm was observed.
Homer Antoniadis et al. [16]	1998	OLED of using fluorine-oxadiazole as emitting and electron-transporting layer, using arylamine as hole-transporting layer.	Luminescent efficiency of blue-light device reached 8.7 cd/A, and the luminous efficiency reached 4.5 lm/W at 200 cd/m ² of emitting intensity.
Junsheng Yu et al. [17]	1999	OLED of using 2,3-dimethyl-8-hydroxyquinoline aluminum as emitting layer and electron-transporting layer, using TPD as hole-transporting layer, using ITO and Mg:Ag as anode and cathode, respectively.	Blue light emitting device with of 5390 cd/m ² emitting intensity was obtained.
M. Heck et al. [18]	2004	Blue-light PLED.	Luminescent efficiency of light device reached 30 cd/A at 100 cd/m ² , life was less than 2000 h, and CIE coordinates of (0.16, 0.38).
Ho Meng-Huan et al. [19]	2007	Deep blue-light OLED.	Luminescent efficiency was 5 cd/A at 20 mA/cm ² , external quantum efficiency reached 4.2 %, the CIE coordinates of (0.15, 0.14), emitting intensity was 100 cd/m ² , the life was 8000 h.
Meng-Ting Lee et al. [20]	2009	Blue-light PLED with double emitting layer.	Luminescent efficiency was 29.5 cd/A, the CIE coordinates of (0.16, 0.35).

tendency to form long-wavelength aggregates/excimers or keto defects in the solid state upon annealing or device operation, and leads to color instability of the light emitted from the fabricated PLEDs [35, 36]. Several approaches have been adopted to suppress this undesirable long wavelength emission, such as copolymerization with anthracene [5, 9], introduction of donor–acceptor (D–A) copolymers units into the main chain [37, 38], end-capping with sterically hindered groups, [27, 29, 39] introduction of bulky substituents at the C-9 position of the fluorene unit [10, 25, 28], and introduction of a chiral structure, have been used to suppress this undesirable long-wavelength emission [21]. These conjugated polymers with enhanced stability have specific optical and physical properties as well as electronic properties.

In this article, we report the design, synthesis, characterization, and device performance of a new conjugated polymer (FPF) containing both electron-transporting oxadiazole moieties and hole-transporting carbazole dendrons units that are functionalized at the C-9 position of fluorene. The characterization results indicated that the FPF is a promising candidate for efficient pure blue emitter.

Experimental

Materials

Carbazole, 1,4-dibromobutane, 2,7-dibromofluorene, 4-(methoxy)benzoic acid hydrazide, 4-tertbutyl benzoyl chloride, phosphorus oxychloride, 1,6-dibromo-hexane, 9,9-dihexyl-2,7-bis(trimethyleneborate)-fluorene, and triethyl phosphate were used as received from J & K Technology Co., Ltd. All other reagents were used as received from Sinopharm Chemical Reagent Beijing Co., Ltd., without any further treatments.

Instruments

¹H-NMR spectra were recorded on a ECA-500 NMR spectrometer (JEOL, Japan, 1H at 600 MHz). Weight-average (M_w) and number-average (M_n) molecular weights were determined by gel permeation chromatography (GPC) under 2.0 mg/mL tetrahydrofuran solution at 30 °C, with four columns (HT3, HT4, HT5, and HT6) series, the THF as mobile phase at a flow rate of 1.0 mL/min, and standard

polybutadiene samples for calibration. Thermo gravimetric analysis (TGA) and differential scanning calorimetry (DSC) measurements were performed on a Mettler-Toledo Star System TGA/DSC simultaneous thermal analyzer from 20 to 250 °C under a nitrogen atmosphere at a heating rate of 10 °C/min. UV absorption spectra were obtained on a Shimadzu UA-2550 spectrophotometer and fluorescence spectra were recorded on a FluoroMax-4 spectrofluorometer with an excitation source of Xe lamp. Photoluminescence (PL) spectrum was measured with a Perkin Elmer LS 55 luminescence spectrometer. The electrochemical behavior of the compounds was investigated by using cyclic voltammetry (CHI 630A Electrochemical Analyzer) with a standard three-electrode electrochemical cell in a 0.1 M solution of tetrabutylammonium tetrafluoroborate in CH₃CN at room temperature, under an atmosphere of nitrogen. The scanning rate was 100 mV/s. A Pt-plate working electrode, a Pt-wire counter electrode, and an Ag/AgNO₃ (0.01 M in CH₃CN) reference electrode were used. The experiments were calibrated with the standard ferrocene/ferrocenium (Fc) redox system under the assumption that the energy level of Fc is 4.8 eV below vacuum.

Device fabrication and measurement

Multiple-layer light-emitting diodes (PLEDs) configured as ITO (Indium tin oxide)/PEDOT:PSS [poly-(3,4-ethylene dioxathiophene) : poly(styrene sulfonate)] (50 nm)/FPF (40 nm)/Alq₃ (8-Hydroxyquinoline aluminum) (20 nm)/LiF:Al (0.5:100 nm) were fabricated for investigation of optoelectronic characteristics. ITO glass substrate with a sheet resistance of 15 Ω □⁻¹ was used. ITO-coated glasses were cleaned consecutively in ultrasonic baths (type: GRANT XUB 10) with acetone and isopropanol (1:10, v/v) for 15 min, according to standard cleaning procedure, an active area of 10 mm² was obtained. After that, ITO-coated glass was dried by high purity N₂ and exposed to UV-ozone for 10 min. A thick hole-transporting layer of PEDOT:PSS was spin-coated (type of Spin coater is TC-218) onto the cleaned ITO-coated glass at a spin speed of 4000 rpm for 30 s. The samples were annealed under nitrogen atmosphere at 150 °C for 15 min to improve the hole injection, the substrate smoothness, and the performance of the PLEDs. The emitting layer was then spin-coated onto the PEDOT:PSS layer from a polymer (FPF) solution in chlorobenzene (1.5 %, w/v, g/mL) at a spin speed of 3000 rpm for 30 s, and the polymer film was treated by thermal annealing at 80 °C for 30 min. Then Alq₃ as emissive layer and electron-transporting layer was deposited (organic molecular beam deposition system, type is OMBD) onto the surface of the FPF' films. Finally, an ultra thin layer of LiF and Al cathode were evaporated (Vacuum coating machine, Beijing Scientific Instrument Factory, type is DM-300B) under high

vacuum by employing shadow mask at a pressure of $\sim 5 \times 10^{-5}$ Pa. The deposition rates were usually 0.5–1 nm/s. The EL spectra, CIE coordinates, and current density–voltage (*J*–*V*) and luminance–voltage (*L*–*V*) characteristics of the devices were measured with a Spectrascan PR650 spectrophotometer in the forward direction, and a computer-controlled Keithley 2400 under ambient conditions at room temperature.

Synthesis of monomers and polymer

The synthesis of monomers and polymer were described in Scheme 1.

9-(4-Bromobutyl)-9H-carbazole (**a**)

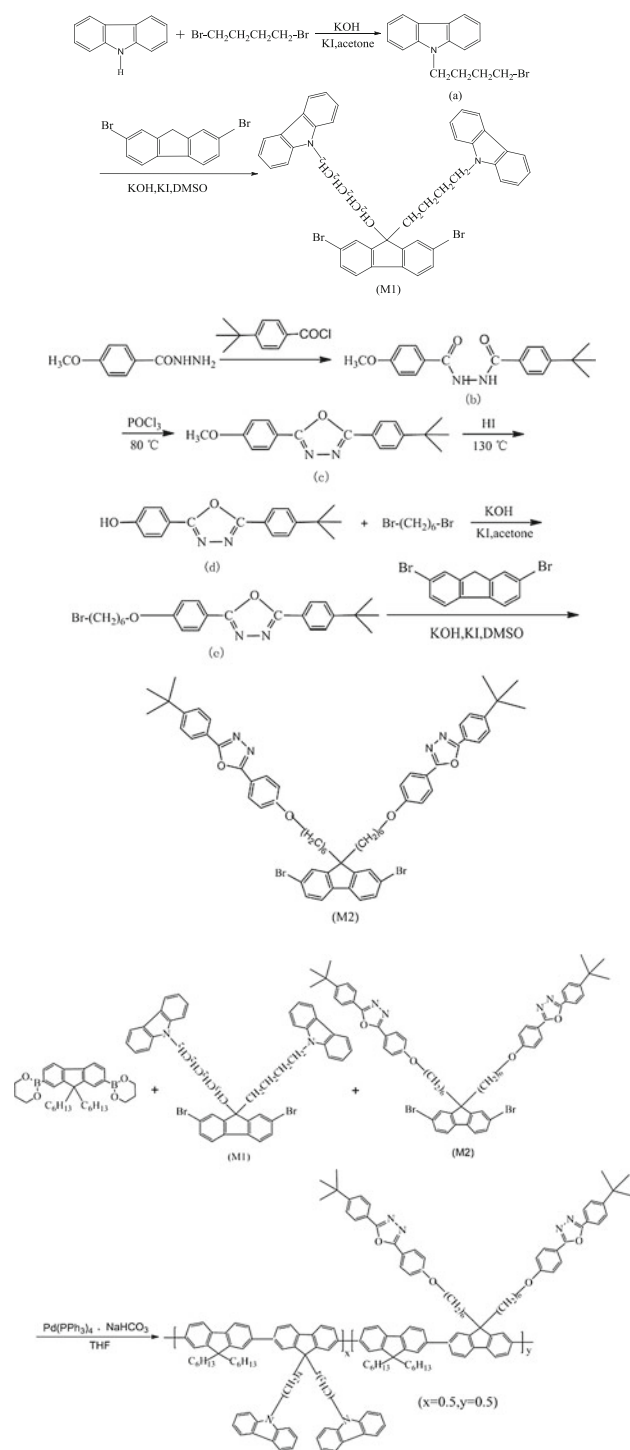
A mixture of carbazole (8.35 g, 50 mmol), KOH (3.36 g, 60 mmol), and KI (0.83 g, 5 mmol) in 50 mL of acetone was added dropwise into a solution of 1,4-dibromobutane (12.96 g, 60 mmol) in acetone (50 mL) in a three-necked flask under magnetic stirring at 60 °C for 6 h. The mixture was rotary evaporated, and the solvent was removed. The crude product was washed with deionized water until a pH of 7 was reached, and it was then dried in vacuo at 60 °C to give solid (**a**) (7.95 g, yield: 52.6 %). The excess 1,4-dibromobutane and other byproducts were removed by recrystallization with ethanol.

The ¹H-NMR (CDCl₃, 600 MHz) δ: ppm 8.08 (s, 2H), 7.46 (d, 2H), 7.38 (d, 2H), and 7.23 (m, 2H) are attributed to fluorene. The 4.34–4.32 (m, 2H), 3.36–3.34 (m, 2H), 2.04–2.02 (m, 2H), and 1.90–1.89 (s, 2H) are attributed to butyl.

2,7-Dibromo-9,9-bis[9-(4-bromobutyl)-9H-carbazole] fluorene (**MI**)

2,7-Dibromo-fluorene (2.58 g, 8 mmol), KI (2.91 g, 18 mmol), KOH (4.45 g, 80 mmol), and dimethyl sulfoxide (DMSO) (25 mL) were mixed in a three-necked flask with a magnetic stirrer and a reflux condenser at 60 °C for 1 h under argon atmosphere. Then a solution of (**a**) (5.28 g, 18 mmol) in DMSO (50 mL) was added dropwise to the three-necked flask under magnetic stirring, and the flask content was refluxed in a reflux condensation at 80 °C for 48 h, under argon atmosphere. After the reaction was complete, the crude product was precipitated from deionized water, filtrated, recrystallized from acetone, and purified by column chromatography on silica gel eluted with ethyl acetate and petroleum ether (10:2, v/v) to give (**MI**) (2.71 g, yield: 43.0 %).

The ¹H-NMR (CDCl₃, 600 MHz) δ: ppm 8.06–8.05 (d, 6H) is attributed to 2,7-dibromofluorene. The 7.42 (s, 8H) and 7.21–7.19 (m, 8H) are attributed to carbazole, and the 4.00–3.98 (m, 4H) and 1.82–0.66 (m, 12H) are attributed to methylene.



Scheme 1 Synthesis routes for monomers and polymer

4-Tertbutylbenzoic acid N'-[4-methoxybenzoyl] hydrazide (b)

4-(Methoxy)benzoic acid hydrazide (9.96 g, 60 mmol), and 4-tertbutyl benzoyl chloride (12.07, 61.25 mmol) were mixed with 200 mL of dioxane in a three-necked flask with

a magnetic stirrer at room temperature for 24 h under argon atmosphere. After the reaction was complete, the crude product was precipitated from deionized water and ether, dried in vacuo to give solid **(b)** (18.85 g, yield: 96.37 %).

The $^1\text{H-NMR}$ (CDCl_3 , 600 MHz) δ : ppm 7.85–7.84 (d, 2H), 7.81–7.80 (d, 2H), 7.49–7.46 (d, 2H), and 6.95–6.93 (d, 2H) are attributed to the phenyl ring; the 3.86 (s, 3H) is attributed to methoxy; the 1.35 (s, 2H) is attributed to amide; and the 1.34 (s, 9H) is attributed to tertbutyl.

2-(4-Tertbutylphenyl)-5-[4-methoxyphenyl]-[1,3,4]oxadiazole (c)

150 mL of phosphorus oxychloride containing **(b)** (15.75 g, 48 mmol) was added into a three-necked flask with a magnetic stirrer at 80 °C for 24 h under argon atmosphere. The mixture was rotary evaporated, and the solvent was removed. The crude product was washed with deionized water, and recrystallized from acetone to give solid **(c)** (11.22 g, yield: 75.4 %).

The $^1\text{H-NMR}$ (CDCl_3 , 600 MHz) δ : ppm 8.08–8.04 (m, 4H), 7.55–7.53 (d, 2H), and 7.04–7.02 (d, 2H) are attributed to the phenyl ring; the 3.89 (s, 3H) is attributed to methoxy; the 1.35 (s, 9H) is attributed to tertbutyl.

2-(4-Tertbutylphenyl)-5-[4-hydroxyphenyl]-[1,3,4]oxadiazole (d)

100 mL of hydrogen periodate (HI) (57 %) containing **(c)** (10 g, 31 mmol) was added into a three-necked flask with a magnetic stirrer at 130 °C for 6 h under argon atmosphere. The mixture was precipitated from a saturated solution of NaCl, filtrated, and recrystallized from acetone to give solid **(d)** (6.57 g, yield: 68.6 %).

The $^1\text{H-NMR}$ (CDCl_3 , 600 MHz) δ : ppm 8.08–8.04 (m, 4H), 7.55–7.50 (d, 2H), and 7.05–7.03 (s, 2H) are attributed to the phenyl ring; the 3.89 (s, 1H) is attributed to hydroxyl, and 1.35 (s, 9H) is attributed to tertbutyl.

2-(4-Tertbutylphenyl)-5-[4-(6'-bromine)-hexyloxyphenyl]-[1,3,4]oxadiazole (e)

Compound **(d)** (5.51 g, 18 mmol), 1,6-dibromo-hexane (5.42 g, 22 mmol), KI (3.68 g, 22 mmol), KOH (10.18 g, 185 mmol), and acetone (150 mL) were mixed in a three-necked flask with a magnetic stirrer at 80 °C for 12 h under argon atmosphere. After cooled to the room temperature, the mixture was extracted with dichloromethane. After removal of the solvent, the residue was dried with anhydrous magnesium sulfate, and the crude product purified by column chromatography on silica gel eluted with THF and petroleum ether (10:2, v/v) to give **(e)** (4.71 g, yield: 57.3 %).

The $^1\text{H-NMR}$ (CDCl_3 , 600 MHz) δ : ppm 8.07–8.04 (t, 4H), 7.55–7.53 (d, 2H), and 7.02–7.01 (d, 2H) are attributed to the phenyl ring; the 4.06–4.04 (t, 2H), 3.58–3.55 (t, 2H), 1.85–1.83 (m, 4H), and 1.62–1.54 (m, 4H) are attributed to hexyloxy; and the 1.37 (s, 9H) is attributed to tertbutyl.

2,7-Dibromo-9,9-bis{2-(4-tertbutylphenyl)-5-[4-(6'-bromine) hexyloxyphenyl]-[1,3,4] oxadiazole} fluorene (M2)

Compound (e) (2.42 g, 5.3 mmol), KOH (2.5 g, 45 mmol), KI (1.2 g, 7 mmol) and DMSO (200 mL) were mixed in a three-necked flask with a magnetic stirrer and reflux condensation at 60 °C for 1 h under argon atmosphere. Then a solution of 2,7-dibromo-fluorene (0.857 g, 2.6 mmol) in 50 mL of DMSO was added dropwise, and the reaction mixture was stirred and condensed in a reflux condenser at 80 °C for 48 h. After the reaction was complete, the crude product was precipitated from deionized water, filtrated, recrystallized from acetone, and purified by column chromatography on silica gel eluted with ethyl acetate and petroleum ether (10:2, v/v) to give (M2) (1.01 g, yield: 41 %).

The $^1\text{H-NMR}$ (CDCl_3 , 600 MHz) δ : ppm 7.83–7.79 (m, 2H), 7.72–7.71 (m, 1H), 7.53–7.51 (m, 1H), and 7.45–7.43 (m, 2H) are attributed to the phenyl ring of 2,7-dibromo-fluorene; the 7.35–7.32 (t, 2H), 7.12–7.07 (t, 1H), 7.02–7.01 (d, 2H), 6.99–6.96 (s, 10H), and 6.86–6.85 (d, 1H) are attributed to the phenyl ring of (e); the 5.01 (s, 2H), 4.31–4.29 (t, 1H), 3.95–3.88 (m, 3H), 2.27 (s, 8H), and 1.46–1.44 (m, 10H) are attributed to methylene; and the 1.44–1.43 (m, 12H) and 1.33 (s, 6H) are attributed to tertbutyl.

Functionalized polyfluorene (FPF)

9,9-Dihexyl-2,7-bis(trimethyleneborate)-fluorene (0.48 g, 1 mmol), (M1) (0.35 g, 0.5 mmol), (M2) (0.38 g, 0.5 mmol), THF (100 mL), sodium bicarbonate (NaHCO_3) (2 g, 20 mmol), deionized water (50 mL), and tetrakis(triphenylphosphine) palladium ($\text{Pd}(\text{PPh}_3)_4$) (0.11 g, 0.1 mmol) were mixed in a three-necked flask with a magnetic stirrer at 60 °C for 48 h under argon atmosphere. The mixture was rotary evaporated, precipitated from methanol, washed for 24 h in a Soxhlet apparatus with petroleum ether to remove trace oligomers and catalyst residues, and filtrated and dried to give the FPF (0.455 g, yield: 47.4 %).

The $^1\text{H-NMR}$ (CDCl_3 , 600 MHz, ppm) spectrum of the FPF is shown in Fig. 1. The detailed structural analysis of the FPF is described in Fig. 1.

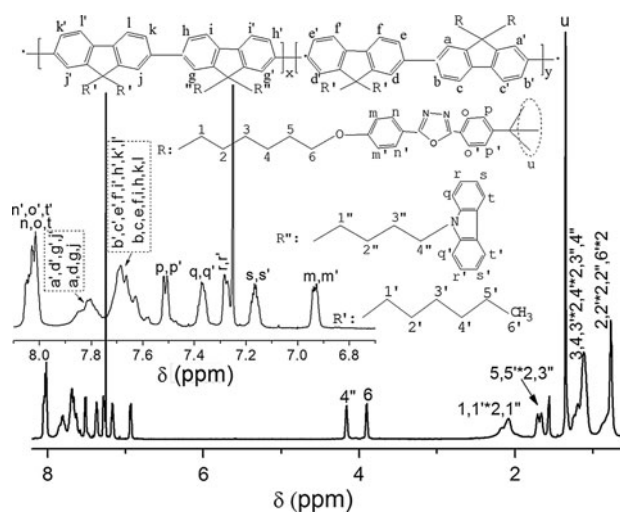


Fig. 1 $^1\text{H-NMR}$ spectrum of FPF

Results and discussion

Synthesis and characterization

The synthesis routes of the monomers and the polymer are shown in Scheme 1. The dendronized derivatives (M1 and M2) were synthesized according to known procedures [29]. (a) and (e) were prepared according to procedures previously described in the literature [33, 40, 41]. (b) and (c) were synthesized according to procedures reported previously [10, 32, 39]. (d) was prepared by Lee et al. [42]. The FPF was obtained by means of the well-known palladium-catalyzed Suzuki coupling reaction [8, 43].

The molecular weights and molecular-weight distributions of the polymer were determined by gel permeation chromatography (GPC). The weight-average molecular weight (M_w) and number-average molecular weight (M_n) were measured to be 71280 and 31185, respectively. The polydispersity index ($\text{PDI} = M_w/M_n$) was calculated to be 2.29. The FPF show good solubility in organic solvents, such as DMF, THF, CHCl_3 , and toluene.

Thermal properties

The thermal properties of the FPF were investigated by using TGA and DSC. The FPF exhibits good thermal stabilities. Figure 2 shows that the thermal decomposition temperature (T_d) of the FPF is around 450–600 °C under nitrogen and the peak thermal decomposition temperature is 495 °C, which is 47 higher than that of the PF shown in the inset of Fig. 2, 38 °C higher than that of the fluorene-co-carbazole polymer [44], and 85 °C higher than that of the dendronized polymer [45].

Figure 3 shows the DSC thermogram of the FPF (the inset shows the DSC curve of the PF). In Fig. 3, curve

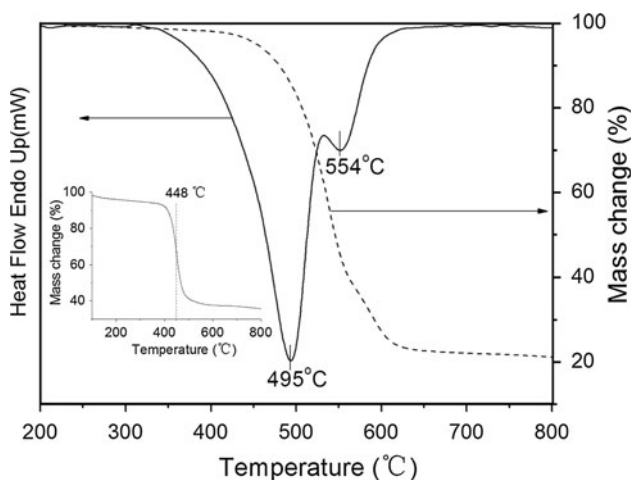


Fig. 2 TGA curve of the FPF (inset: TGA curve of PF)

(a) represents the first heating run from 25 to 300 °C. An exothermic peak appears at 104 °C is associated with the crystallization of the sample. As the sample is heat further, endothermic peaks appear at 176 and 195 °C because of the increase in thermal motion of the molecules above 176 °C as the sample melts. There are two possible explanations for the two melting peaks: first, the sample may contain impurity; second, the sample may contain different configurations of polymer chains. The melted sample was cooled rapidly in liquid nitrogen into an amorphous glassy state. Further heating of the sample from room temperature results in curve (b). A small endothermic peak appears at 160 °C, which is the glass transition temperature (T_g) of the FPF. The T_g of the polymer is higher than that of PF (138 °C, see inset of Fig. 3) and that of the PFCO1 (101 °C, see reference [37]) [45], probably because of the higher molecular weight of the FPF and steric effect

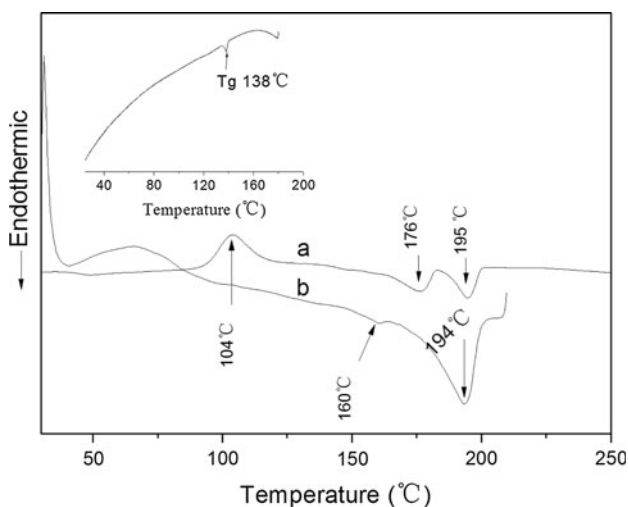


Fig. 3 DSC curve of the FPF (inset: DSC curve of the PF)

of the dendron side chains. Thus, the incorporation of carbazole and oxadiazole functional dendronized units into the main chains has successfully increased the T_g of the PF. The improved T_g is very important for the use of these polymers as emissive materials in EL displays [46].

Optical properties

Figure 4 displays the UV and PL spectra of the FPF in a film spin coated from dilute CHCl_3 solution. The FPF shows a UV absorption band in the 320–410 nm range. The shorter absorption maximum at 347 nm is due to the absorption of the carbazole and oxadiazole peripheral groups. The additional absorption peak of FPF at 374 nm is attributed to the $\pi-\pi^*$ transition associated with the conjugated polymer backbone. The absorption onset wavelength of FPF film is determined to be 423 nm, which gives rise to the corresponding optical band gap ($E_g = 1240/\lambda_{\text{onset}}$) [47] of 2.93 eV. As shown in the inset in Fig. 4, the E_g of PF is 2.92 eV. Moreover, the green emission of PF is very obvious. A comparison of the PL emission spectra of PF and FPF shows that the green emission of FPF is effectively reduced by the functionalized side chains. The large shielding effect of the dendronized carbazole and oxadiazole side chains has efficiently suppressed the aggregation of polymer main chains to increase pure blue emission.

At the same time, the main PL emission peak of FPF is located at 421 nm, with a shoulder at 442 nm. The emission at shorter wavelengths originates from the PF segments, whereas, the band at longer wavelengths can be attributed to the carbazole chromophores [44]. In particular, FPF can emit 380–440 nm pure blue.

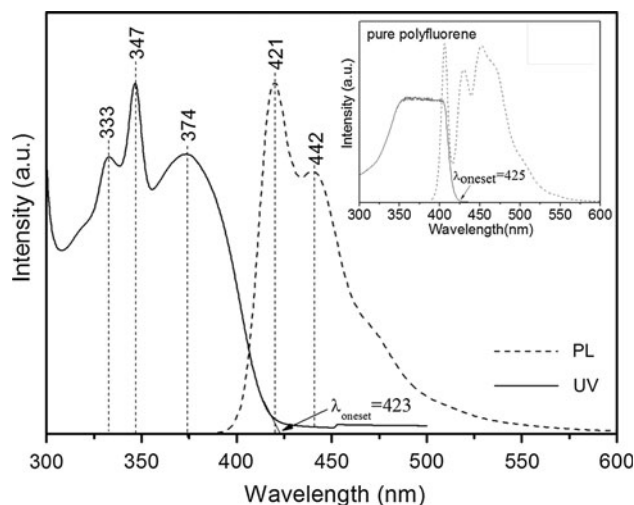


Fig. 4 UV and photoluminescence (PL) spectra (excitation wavelength = 380 nm) of the FPF in the film

Electrochemical properties

To appropriate the energy band structural scheme of the ITO/PEDOT:PSS (50 nm)/FPF (40 nm)/Alq₃ (20 nm)/LiF:Al (0.5:100 nm) (PLED device), it is necessary to determine the energy levels of the highest occupied molecular orbital (HOMO) and the lowest unoccupied molecular orbital (LUMO) of the FPF. CV was used to investigate the redox behavior of the FPF thin films. The potential estimated here was based on the reference energy level of ferrocene (4.8 eV below the vacuum level) according to the following equations: [48]

$$E_{\text{HOMO}} = -e[E_{\text{on}}^{\text{ox}} + (4.8 - E_{\text{ref}})](eV) \tag{1}$$

where $E_{\text{on}}^{\text{ox}}$ is the onset oxidation potential of the FPF versus Ag/Ag^+ and E_{ref} is the formal potential of the ferrocene/ferrocenium ($\text{F}_\text{C}/\text{F}_\text{C}^+$) reference against Ag/Ag^+ (E_{ref} was measured to be 0.09 V). $E_{\text{on}}^{\text{ox}}$ was measured to be 1.00 V (see Fig. 5a). From Eq. (1), E_{HOMO} of FPF was calculated to be -5.71 eV. E_{LUMO} was calculated by using the following equation:

$$E_{\text{LUMO}} = E_{\text{HOMO}} + E_g \tag{2}$$

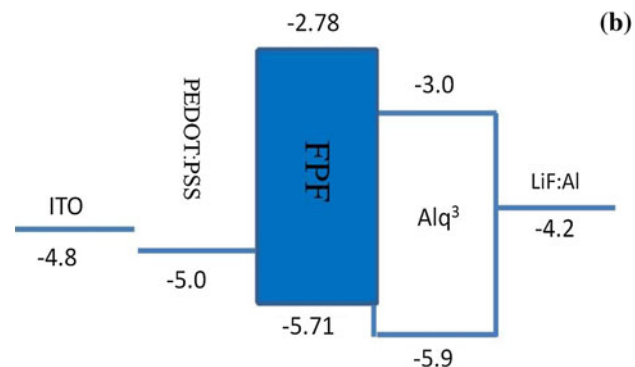
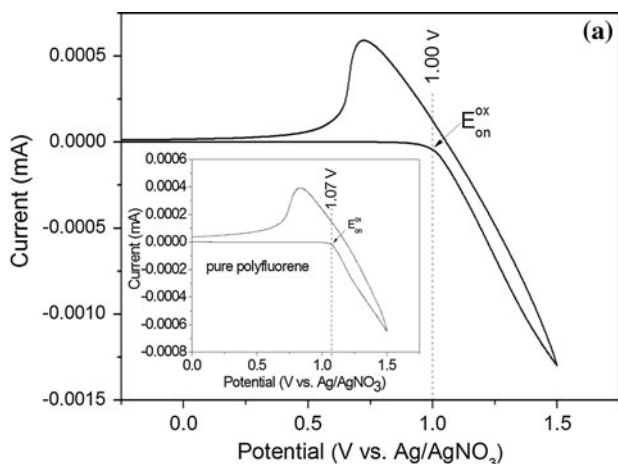


Fig. 5 **a** Cyclic voltammogram of FPF in film and **b** Energy band diagram of ITO/PEDOT:PSS (50 nm)/FPF (40 nm)/Alq₃ (20 nm)/LiF:Al (0.5:100 nm)

where E_g is the energy gap (optical band gap), estimated to be 2.93 eV from the edge of the UV absorption band of the film (see Fig. 4). From Eq. (2), E_{LUMO} of FPF was calculated to be -2.78 eV. The energy band diagram of the PLED device is shown in the Fig. 5b. From the inset in Fig. 5a, $E_{\text{on}}^{\text{ox}}$ of PF was measured to be 1.07 eV. From Eq. (1), E_{HOMO} of PF was calculated to be -5.78 eV. From Eq. (2), E_{LUMO} of PF was calculated to be -2.86 eV. It is obvious that the bipolar nature of the carbazole and oxadiazole system can help to raise the HOMO energy level and the LUMO level of the emitting material. Therefore, the good electronic properties afforded by the dendronized functional carbazole and oxadiazole side chains can give rise to efficient injection and transport of holes and electrons.

Electroluminescence (EL) properties

A PLED device was fabricated to determine the EL prosperity of the FPF. Figure 6a shows the EL spectra at different currents for the PLED device. At currents of 1, 2, and 4 mA, the majority of the EL is located in the blue region. But the EL spectra red shifts as the current increases to 10 mA, as a result of the thermal effect under large currents. The green emission from the PF is not observed in the device. The large shielding effect of the dendronized carbazole and oxadiazole side chains has efficiently suppressed the aggregation of polymer main chains to give rise to the more pure blue emission. The inset in Fig. 6a is a digital photograph of the device based on FPF. We can see that the device emits pure blue light, in accordance with the EL spectra.

The EL spectrum of FPF is similar to PL spectrum, an indication that the EL emissions originate from the polymer, and are not affected by the addition of PEDOT and Alq₃.

The emission spectra can be characterized by their Commission Internationale de L'Eclairage (CIE) 1931 chromaticity coordinates (x, y) at different turn-on voltages, as shown in Fig. 6b, in which x ranges from 0.16 to 0.2 and y ranges from 0.12 to 0.21. Here shows the pure blue light emission.

The luminance–voltage (L – V) and current density–voltage (J – V) characteristics of the PLED device shown in Fig. 7 indicates that the luminance and current density increase exponentially with the increase in forward bias voltage. This behavior is typical of diodes. The PLED device exhibits a maximum luminance of 980 cd/m^2 at the voltage of 13.0 V, and a maximum current density of 726 mA/cm^2 at the voltage of 14.4 V. Moreover, the J – V curve indicates that the turn-on voltage of the PLED device is 8.54 V. The low electron mobility of a PLED

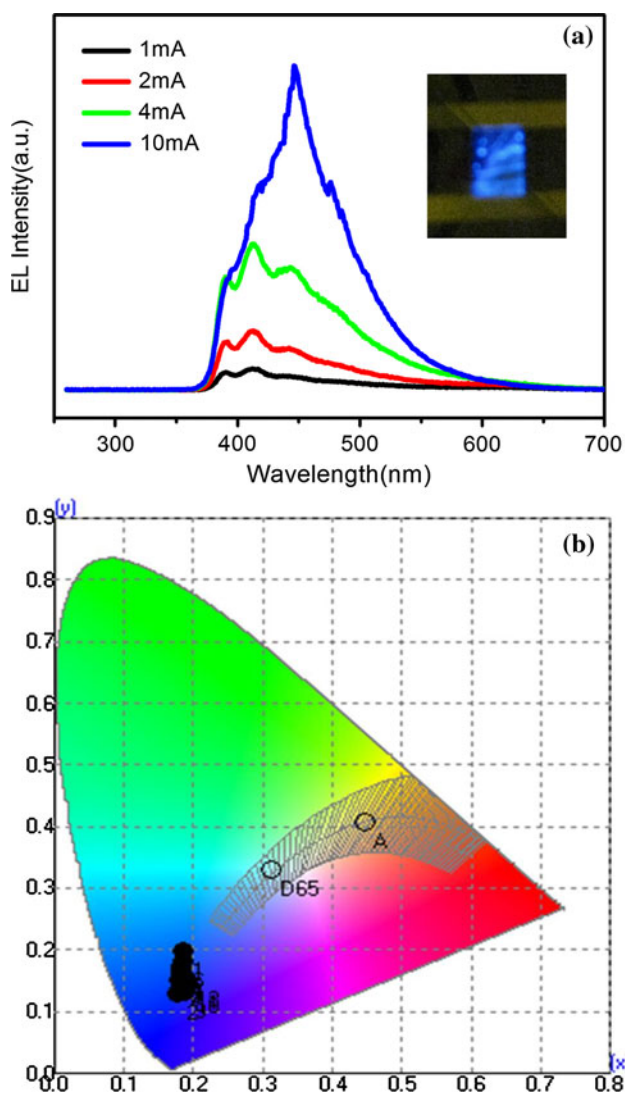


Fig. 6 **a** Electroluminescence (EL) spectra at different currents and **b** CIE spectra of ITO/PEDOT:PSS (50 nm)/FPF (40 nm)/Alq₃ (20 nm)/LiF:Al (0.5:100 nm)

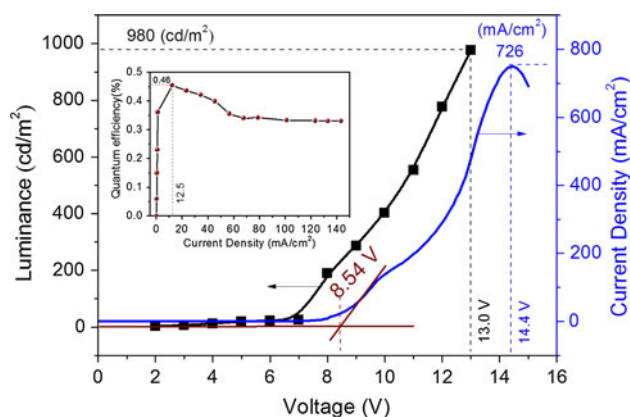


Fig. 7 Luminance–voltage (L – V) and current density–voltage (J – V) characteristics of ITO/PEDOT:PSS (50 nm)/FPF (40 nm)/Alq₃ (20 nm)/LiF:Al (0.5:100 nm)

device limits the efficient recombination of holes and electrons, resulting in a decrease in EL efficiency. The maximum EL efficiency of the PLED device based on FPF is 0.46 % at the current density of 12.5 mA/cm², as shown in the inset.

Conclusions

A blue light-emitting conjugated polymer (FPF) has been successfully synthesized by the palladium-catalyzed Suzuki coupling reaction. The chemical structures determined by ¹H-NMR and FTIR are in agreement with the expected chemical structures. GPC and CV results indicate that the FPF has high molecular weight and is an electrochemically stable amorphous material. TGA and DSC show excellent thermal stability ($T_d > 450$ °C) and high glass transition temperature ($T_g = 160$ °C). Devices of the FPF emit deep blue-light with CIE coordinates of (0.16–0.2, 0.12–0.21). The maximum luminance and current density of FPF were found to be 980 cd/m² and 726 mA/cm², respectively. The maximum EL efficiency of the device based on FPF is measured to be 0.46 %, at the current density of 12.5 mA/cm². The good EL properties afforded by the dendronized functional carbazole and oxadiazole side chains can give rise to efficient injection and transport of holes and electrons. The FPF could be a promising candidate for blue-light-emitting polymers.

Acknowledgements This study was supported by the National Natural Science Foundation of China (50903079), and Foundation of Beijing Institute of Aeronautical Materials (KF53100302).

References

1. Wang P, Chai CP, Yang Q, Wang FZ, Shen ZH, Guo HQ et al (2008) *J Polym Sci A* 46:5452
2. Wu FI, Reddy DS, Shu CF (2003) *Chem Mater* 15:269
3. Ye T, Zhu M, Chen J (2012) *J Mater Chem* 22:6413
4. Ye L, Chen ZK, Ye TL (2010) *Polymer* 51:1270
5. Liu J, Cao JX, Shao SY, Xie ZY, Cheng YX, Geng YH et al (2008) *J Mater Chem* 18:1659
6. Chen RT, Chen SH, Hsien BY, Chen Y (2009) *J Polym Sci A* 47:2821
7. Gu C, Dong WY, Yao L, Lv Y, Zhang ZB, Ma YG (2012) *Adv Mater* 24:2413
8. Huang F, Zhang Y, Liu MS, Cheng YJ, Jen AKY (2007) *Adv Funct Mater* 17:3808
9. Guo X, Yao B, Jiang GX, Cheng YX, Xie ZY, Wang LX et al (2008) *J Polym Sci A* 46:4866
10. Zhan XW, Liu YQ, Wu X, Wang S, Zhu DB (2002) *Macromolecules* 35:2529
11. Peng Q, Xu J, Li MJ, Zheng WX (2009) *Macromolecules* 42:5478
12. Park JH, Koh TW, Do Y, Lee MH, Yoo S (2012) *J Polym Sci A* 50:2356
13. Vincett PS, Bbarlow WA, Hann RA, Roberts GG (1982) *Thin Solid Films* 94:171

14. Adachi C, Tetsui T, Saito S (1990) *Appl Phys Lett* 56:799
15. Yu-guang Ma, Jian-guo T, Shi-yong L, Jia-cong S (1994) *Chin Sci Bull* 39:1070
16. Antoniadis H, Inbasekaran M, Woo EP (1998) *Appl Phys Lett* 73:3055
17. Junsheng Yu, Chen Z, Sakuratani Y, Suzuki H, Tokita M, Miyata S (1999) *Jpn J Appl Phys* 38:6762
18. Heck M, Brown JJ (2004) *Inf Disp* 20:12
19. Meng-Huan H, Yao-Shan W, Shih-Hen W, Teng-Ming C (2007) *Appl Phys Lett* 91:083515
20. Lee M-T, Lin J-S, Chu M-T, Tseng M-R (2009) *Appl Phys Lett* 94:083506
21. Usluer O, Demic S, Egbe DAM, Birckner E, Tozlu C, Pivrikas A et al (2010) *Adv Funct Mater* 20:4152
22. Zou YP, Zhou Y, Wu GL, Li YF, Pan CY (2009) *J Appl Polym Sci* 111:978
23. Jung IH, Jung YK, Lee J, Park JH, Woo HY, Lee JI et al (2008) *J Polym Sci A* 46:7148
24. Huang ST, Liaw DJ, Hsieh LG, Chang CC, Leung MK, Wang KL et al (2009) *J Polym Sci A* 47:6231
25. Chu Z, Wang D, Zhang C, Fan X, Tang YW, Chen L et al (2009) *Macromol Rapid Commun* 30:1745
26. Setayesh S, Grimsdale WT, Enkelmann V, Mullen K, Meghdadi F et al (2001) *J Am Chem Soc* 123:946
27. Shu CF, Dodda R, Wu FI, Liu MS et al (2003) *Macromolecules* 36:6698
28. Wu FI, Shih PI, Shu CF (2005) *Macromolecules* 38:9028
29. Wu CW, Tsai CM, Lin HC (2006) *Macromolecules* 39:4298
30. Wu CW, Lin HC (2006) *Macromolecules* 39:7232
31. Zhou XH, Niu YH, Huang F, Liu MS et al (2007) *Macromolecules* 40:3015
32. Tsai LR, Chen Y (2007) *Macromolecules* 40:2984
33. Jin Y, Kim JY, Park SH, Kim J, Lee S, Lee K et al (2005) *Polymer* 46:12158
34. Chen RT, Su WF, Chen Y (2011) *J Polym Sci A* 49:184
35. Zhen CG, Dai YF, Zeng WJ, Ma Z, Chen ZK et al (2011) *Adv Funct Mater* 21:699
36. Ji JH, Wan JH, Huang W (2008) *Sci China Ser B* 51:497
37. Zhang MJ, Guo X, Wang XC, Wang HQ, Li YF (2011) *Chem Mater* 23:4264
38. Shi SW, Jiang P, Chen S, Sun YP, Wang XC, Wang K et al (2012) *Macromolecules* 45:7806
39. Sung HH, Lin HC (2004) *Macromolecules* 37:7945
40. Xia CJ, Rigoberto CA (2001) *Chem Mater* 13:1682
41. Yang SH, Huang CH, Chen CH, Hsu CS (2009) *Macromol Chem Phys* 210:37
42. Lee YZ, Chen XW, Chen SA, Wei PK, Fann WS (2001) *J Am Chem Soc* 123:2296
43. Li Y, Ding J, Day M, Tao Y, Lu JP, Marie D (2004) *Chem Mater* 16:2165
44. Yang C, Song HS, Liu DB (2012) *J Mater Sci* 47:3315. doi: [10.1007/s10853-011-6170-8](https://doi.org/10.1007/s10853-011-6170-8)
45. Peng Q, Li MJ, Lu SQ, Tang XH (2007) *Macromol Rapid Commun* 28:785
46. Tokito S, Tanaka H, Noda K, Okada A, Taga Y (1997) *Appl Phys Lett* 70:1929
47. Wang XC, Wang HQ, Yang Y, He YJ, Zhang L, Li YF et al (2010) *Macromolecules* 43:709
48. Wang XC, Sun YP, Chen S, Guo X, Zhang MJ, Li XY et al (2012) *Macromolecules* 45:1208